

## A rigorous framework for detecting SARS-CoV-2 spike protein mutational ensemble from genomic and structural features



Saman Fatihi<sup>a,b,1</sup>, Surabhi Rathore<sup>a,b,1</sup>, Ankit K. Pathak<sup>a</sup>, Deepanshi Gahlot<sup>a,b</sup>,  
Mitali Mukerji<sup>a,b,2</sup>, Nidhi Jatana<sup>a</sup>, Lipi Thukral<sup>a,b,\*</sup>

<sup>a</sup> CSIR-Institute of Genomics and Integrative Biology, Mathura Road, New Delhi, 110 025, India

<sup>b</sup> Academy of Scientific and Innovative Research (AcSIR), CSIR-Human Resource Development Centre, (CSIR-HRDC), Kamla Nehru Nagar, Ghaziabad, 201002, Uttar Pradesh, India

### ARTICLE INFO

Handling editor: Chandra Shekhar Verma

#### Keywords:

SARS-CoV-2  
Spike protein  
Mutations  
Lineages  
Structural features

### ABSTRACT

The recent release of SARS-CoV-2 genomic data from several countries has provided clues into the potential antigenic drift of the coronavirus population. In particular, the genomic instability observed in the spike protein necessitates immediate action and further exploration in the context of viral-host interactions. By temporally tracking 527,988 SARS-CoV-2 genomes, we identified invariant and hypervariable regions within the spike protein. We evaluated combination of mutations from SARS-CoV-2 lineages and found that maximum number of lineage-defining mutations were present in the N-terminal domain (NTD). Based on mutant 3D-structural models of known Variants of Concern (VOCs), we found that structural properties such as accessibility, secondary structural type, and intra-protein interactions at local mutation sites are greatly altered. Further, we observed significant differences between intra-protein networks of wild-type and Delta mutant, with the latter showing dense intra-protein contacts. Extensive molecular dynamics simulations of D614G mutant spike structure with hACE2 further revealed dynamic features with 47.7% of mutations mapping on flexible regions of spike protein. Thus, we propose that significant changes within spike protein structure have occurred that may impact SARS-CoV-2 pathogenesis, and repositioning of vaccine candidates is required to contain the spread of COVID-19 pathogen.

### 1. Introduction

The current novel coronavirus disease 2019 (COVID-19) outbreak is caused by severe acute respiratory syndrome coronavirus 2 (SARS-CoV-2) (Andersen et al., 2020). By August 2021, the World Health Organization (WHO) reported 207,784,507 confirmed cases with 4,370,424 deaths all over the world. Global sequencing initiatives have been indispensable in understanding SARS-CoV-2 genomic diversity. There is a great deal of interest in identifying how spike protein of SARS-CoV-2 is evolving as it directly interacts with the human ACE2 (hACE2) receptor (Walls et al., 2020). Efforts to understand mutations and predict associated pathogenesis have been hampered by our inability to evaluate combinations of mutations.

The spike protein has multidomain structural architecture and comprises S1 and S2 subunits (Walls et al., 2020). The viral infection

commences upon binding of the S1 subunit to the hACE2, followed by the proteolytic cleavage in the spike protein resulting in the dissociation of the S1 and S2 subunits, further leading to membrane fusion and virus entry inside the cell (Hoffmann et al., 2020b). S1 subunit is the key domain responsible for mediating the receptor binding and hence is considered to be the potential target for vaccines and drugs against COVID-19 (Lan et al., 2020; Dai and Gao, 2021; Wang et al., 2021c). S1 subunit (1–685 a.a.) is comprised of a signal peptide followed by the N-terminal domain (NTD), and the receptor-binding domain (RBD) (Walls et al., 2020). Although the function of the NTD is not clearly known, it has been suggested to harbor the neutralizing epitopes (Chi et al., 2020; Liu et al., 2020; Graham et al., 2021). The RBD is a well-established domain that is characterised into a receptor-binding motif (RBM) and the core region (Mittal et al., 2020; Shang et al., 2020). Residues of the RBM play an important role in mediating key

\* Corresponding author. CSIR-Institute of Genomics and Integrative Biology, Mathura Road, New Delhi, 110 025, India.

E-mail address: [lipi.thukral@igib.res.in](mailto:lipi.thukral@igib.res.in) (L. Thukral).

<sup>1</sup> Co-first authors.

<sup>2</sup> Presently at: Dept of Bioscience and Bioengineering, Indian Institute of Technology (IIT), Jodhpur, India.

interactions with the hACE2 receptor (Lan et al., 2020). Many RBD targeting antibodies interfere either with RBD-hACE2 binding or inhibit the RBD to acquire the up conformation (Chen et al., 2020; Barnes et al., 2020; Ju et al., 2020). Recent studies on monoclonal antibody response against mRNA vaccines have shown a co-dominant antibody binding to the NTD and RBD, thereby making NTD an equally important therapeutic target (Amanat et al., 2021). Another interesting functional motif is the connecting linker region between the RBD and HR1 that contains two critical furin cleavage sites, namely- S1/S2 site and S2' followed by a fusion peptide (Xia et al., 2020; Hoffmann et al., 2020a). The understanding of these regions and how they are evolving during the current pandemic is critical for enhancing present vaccine efficacy.

Early analysis of viral variants revealed a single amino acid substitution D614G, which has now become a widespread dominant variant (Korber et al., 2020). Although it did not reveal greater clinical severity, structural features of mutant D614G spike showed interesting characteristics (Volz et al., 2021; Groves et al., 2021). The conformational state of spike protein was found more stable in an “up” conformation (Yurkovetskiy et al., 2020). In Oct 2020, multiple co-occurring mutations in the SARS-CoV-2 within spike protein were reported (Rees-Spear et al., 2021). Three major lineages, including B.1.1.7 (Alpha), B.1.351 (Beta), and P.1 (Gamma) were seen emerging in patients from the UK, South Africa, and Brazil, respectively (Rambaut et al., 2020; Tegally et al., 2020; Resende et al., 2021), which are now classified as the VOCs. Compared to previous variants, the Alpha variant raised concern due to the presence of N501Y mutation in the RBD of the spike protein. Particularly in spike, this variant emerged with several other mutations like 69/70 deletion and P681H mutation present in the N-terminal domain (NTD) and near S1/S2 site, respectively (Rambaut et al., 2020). Another variant from South Africa (B.1.351) emerged independently with multiple mutations in the RBD (K417N and E484K) along with N501Y, however, lacked the 69/70 deletion mutations in the NTD segment (Tegally et al., 2021). The lineage B.1.526 is classified as a Variant of Interest (VOI) which have multiple spike mutations with unique substitutions L5F, T95I, and, D253G, which were not present earlier in any other lineages (Annavejhalala et al., 2021; West Jr et al., 2021). Recently, a rapidly transmitting variant emerged in India, namely-B.1.617.2 (Delta) with unique RBD mutations E484Q and L452R, two deletions (E156del and F157del) and a substitution (R158G) in the NTD, and 4 other mutations including D614G (Kannan et al., 2021). A sub-lineage of Delta with an additional mutation, K417N is termed as AY.1 (Delta-plus). Interestingly, each lineage contains more than a handful of spike mutations also present on non-RBD regions. Although they are not the focus of extensive characterisation, they are likely to contribute in a specific manner towards spike evolution. A better structural understanding of the pattern underlying these lineages, as a whole will facilitate in predicting the immune response with new SARS-CoV-2 variants.

In this work, we integrated large-scale genomic variations of SARS-CoV-2 spike protein with extensive structural characterisation. We identified mutational hotspots based on a temporal acquisition of mutations and found distinct variant and invariant patches distributed throughout the structure. The contribution of lineage-defining mutations was evaluated domain-wise to understand structural motifs that are accumulating more mutations than others. Some of these mutations have also evolved into VOCs. Based on mutated structural models of known VOCs, we found that structural properties such as accessibility, secondary structural type, and intra-protein interactions at local mutation sites are greatly altered. Extensive molecular dynamics simulations of the D614G mutant spike structure with hACE2 further revealed dynamic features that may play a key role in the conformational ensemble of the spike protein. Our results support the view that structural changes of prominent SARS-CoV-2 lineages significantly alter structural properties of spike protein and hence may require updating spike-based vaccine candidates.

## 2. Results

### 2.1. Genomic diversity of spike protein

We present meta-analysis of SARS-CoV-2 genomic data from GISAID sampled until May 2021. Amino acid substitutions, including missense and deletions/insertions were extracted for the spike protein. In total, 6517 mutations were observed in 1,624,465 spike sequences. The frequency of each substitution was mapped onto the full-length spike structure model as shown in (Fig. 1). Both S1 and S2 subunits are marked, with the S1 domain of the SARS-CoV-2 consisting of the N-terminal domain (NTD: 14–305 a.a.) and the receptor binding domain (RBD: 319–541 a.a.) clearly accumulating more mutations. The S1 subunit harbours the prominent D614G mutation present in 99.84% of genomes (Isabel et al., 2020). The sequence alignment conservation with spike protein homologs also revealed that the S1 subunit is highly variable compared to the S2 stalk, with the HR1 region as the most conserved segment (Fig. S1). While the majority of residues show low-frequency mutation rate, two major frequency groups were observed. Eight prominent mutations were present in the first group with more than 50% frequency; N501Y, P681H, T716I, D1118H, A570D, S982A, HV69/70del, and Y144del. The second group with a frequency between 1 and 20% displayed 32 unique residues, with 53% and 18% amino acids present in the NTD and RBD domains, respectively. We thus, were able to associate mutations with structural domains and next utilized large-scale genomic data to understand the domain-wise temporal acquisition of mutations.

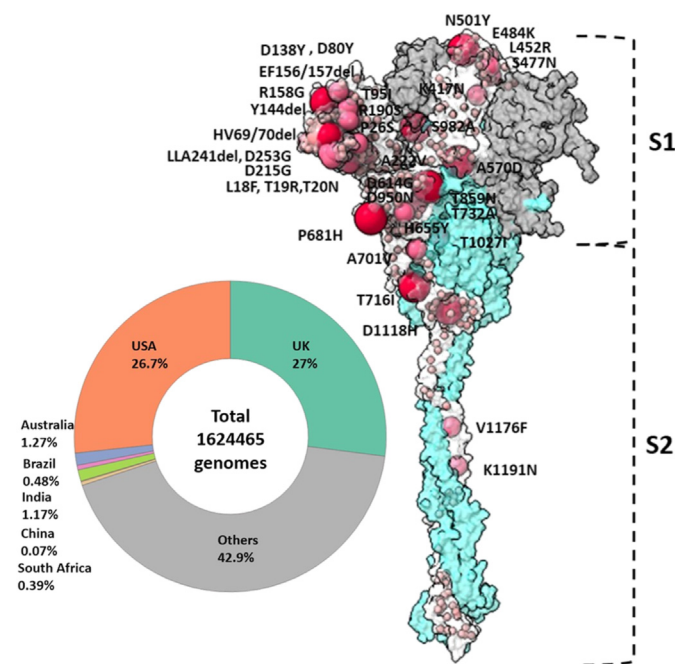


**Fig. 1. Genomic Diversity of SARS-CoV-2 spike protein.** In total, 1,624,465 genomes were retrieved from GISAID, as plotted in the pie chart, with different colors showing country-wise submitted genomes till May 2021. The modeled full-length spike protein is shown in surface representation, with the S1 and S2 subunit colored in grey and cyan, respectively. In total, 6517 mutations were mapped on one protomer, out of which 1312 were found to be on unique sites. The size of the sphere indicates frequency of mutations, with dark to low gradients showing a higher to lower frequency range. The amino acids mutating at higher frequency are marked in text. (For interpretation of the references to colour in this figure legend, the reader is referred to the web version of this article.)

## 2.2. Temporal analysis of mutational hotspots reveals hypervariable regions on spike protein

How did distinct protein regions evolve since the start of the covid-19 pandemic? To answer this, we located high-frequency mutations (>1% frequency) on the spike structure to understand the invariant and variant patches on different spike domains. Not all residue positions are susceptible to mutations. A clear trend emerging from dynamic tracking of genomic data is the constant evolution of specific S1 domains in the NTD, RBD, and linker regions (Fig. 2A; Fig. S2). In early pandemic, L5F substitution in the signal peptide was present, along with D614G mutation in the linker. From July 2020, a noticeable accumulation of mutations was observed in the NTD and RBD regions. The S2 stalk showed least number of mutations, with three variable segments, specifically the L1 region (701–716 a.a.), S982 residue in the HR1, and D1118 residue in the loop region connecting HR1 and HR2 region.

To look at deeper level, a quantitative description of the time progression of highly variable S1 domain regions is shown in Fig. 2B. Within the NTD, five prominent variant stretches were observed, with Y144 deletion, G142D, E156-F157 deletion, and R158G segment as the largest contiguous patch. The N-terminal region of the NTD, namely L18F, T19R,

T20N, evolved early during the pandemic. Later during the pandemic, several segments in N1, N3, and N5 loops of NTD mutated significantly faster, indicating that these regions are hypervariable segments, also shown as protein snapshots. Interestingly, the connecting region between the NTD and RBD (N2R: 310–319) is not mutating. While the core of the RBD consisting of five stranded antiparallel  $\beta$ -sheet is an invariant region, the RBM motif that binds to the hACE2 receptor harbored 99% of the RBD mutations. Only a single K417 residue is present outside the RBM, however, it is still at the interface and is known to form a salt bridge with D30 of the hACE2 receptor. The linker region consists of variant stretches contributed from three prominent mutations A570D, H655Y, and P681 H/R along with D614G. Overall, spike protein harbors multiple prevalent mutations which form mutational clusters that have relatively evolved more than others. Apart from the well-characterised functional significance of RBM, previous reports have also characterised NTD as a major antibody epitope. We speculate that these protein regions are important for the function or stability of protein and hence are under greater selective pressure. In a recent study, a collection of SARS-CoV-2-neutralizing antibodies reveal significant antibodies directed against the NTD, and the most potent were targeted at the 2–51 patch on the NTD. (Liu et al., 2020; McCallum et al., 2021; Chi et al., 2020). We

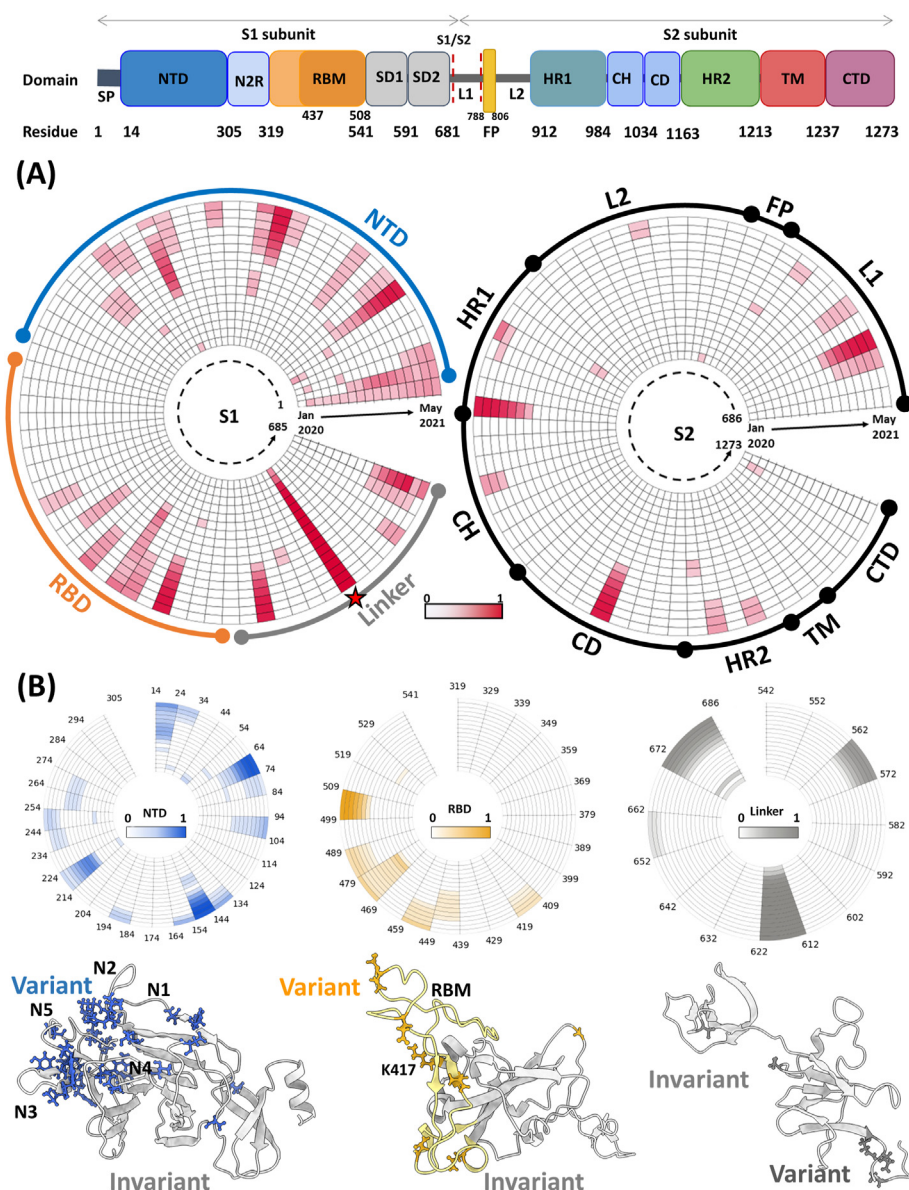


**Fig. 2. Mutation clusters of SARS-CoV-2 spike protein.** (A) The schematic view of the domain architecture of SARS-CoV-2 spike protein is shown in the top row. The circular plot shows the ‘normalised mutation frequency’ in a time-dependent manner. Each row represents one month and, in total 17-month period from January 2020 to May 2021 is shown. The spike protein of 1273 residues is divided into 129 ten-residue bins and is shown for S1 and S2 subunits separately. The normalised mutation frequency is calculated as the ratio of  $N_i$  and  $N_{ref}$ . The  $N_i$  refers to cumulative number of mutations from global GISAID data for each bin and  $N_{ref}$  is the bin that corresponds to maximum frequency bin. The color gradient of red denotes the intensity of mutation frequency, with 1 being the highest. The D614G present in the linker region is marked as a star for reference as it is now present in  $\approx 98\%$  of the genomes. (B) Zoomed in circular plots are shown for three major parts of the S1 subunit; NTD, RBD, and Linker regions. The corresponding structural mapping for each domain is shown to depict mutational spots. The mutation site is depicted in stick representation highlighting the variant patches. (For interpretation of the references to colour in this figure legend, the reader is referred to the web version of this article.)



speculate that collectively these protein regions are important for the function or stability of protein and hence are under greater selective pressure.

### 2.3. Integrating defining spike mutations within lineages reveal coaxiality at NTD

SARS-CoV-2 is continually evolving and population genomics studies reveal constellation of mutations that define a particular lineage. In principle, lineages reveal pool of mutations that is characteristic of subset of viral population. To gather insights on co-occurring mutations, we obtained lineage information of SARS-CoV-2 from the PANGOLIN database. Fig. 3A shows the time evolution of 43 SARS-CoV-2 lineages. Strikingly, number of spike mutations have significantly increased since evolution of B.1.1.7 lineage in October 2020 (Fig. S3). For instance, the recent Delta lineage accumulated a total of 9 defining spike mutations throughout the protein.

The lineage data also allowed us to examine the underlying link of co-occurring mutations with the structural domains. For example, are these co-occurring mutations emerging in a specific pattern? We identified that lineage-defining mutations were maximally located on the NTD region followed by RBD, Linker, S2 subunit, and signal peptide (Fig. 3B). In particular, 5 NTD residues appeared in combination that persisted in multiple lineages. On the other hand, fewer RBD residues were involved. A deeper understanding of residue-wise distribution showed that specific domain combinations were preserved in six major lineages, including five VOCs. We observed that the majority of the combinations occur within four domains, with NTD as a key co-occurring domain (Fig. 3C). For instance, L18F, T20N, P26S, D138Y, and R190S are present in P.1 lineage. Similarly, the recent B.1.617.2 lineage possess 4 NTD mutation combination (T19R, E156del, F157del, and R158G). The RBD residues,

on the other hand, utilise less number of mutations that have overlapped with number of lineages. A single amino acid substitution L452R is present in multiple lineages, including B.1.526, B.1.427, B.1.429, B.1.617.1, B.1.617.3, and lineages designated as Delta (B.1.617.2, AY.1, AY.2, and AY.3). Similarly, E484K is present in B.1.525 (Eta), P.1 (Gamma), and B.1.351 (Beta). The combination of K417N, E484K, and N501Y substitutions was also present in B.1.351 (Beta) and P.1 (Gamma). The linker region with P681R and H655Y along with D614G were the main amino acid co-occurring substitutions. In addition, NTD also has more intra-domain mutation combinations across VOC lineages.

Overall, there exists a pattern of mutational clusters with the highest fraction of inter-domain combinations mapping to the NTD-RBD, NTD-linker, and NTD-S2 regions. These results indicate that NTD forms a co-axial cluster that is under stronger selective pressure than other domains.

### 2.4. Structural determinants of mutations in VOCs reveal higher accessibility and disordered loops

Are these co-occurring mutations altering the spike topology or its interface that may impact versatility of protein interactions? In order to understand molecular level details, we generated six glycosylated spike protein models for key lineages (Fig. 4A). These structures now provide us with spatial maps that include amino acid substitutions and in some cases deleted segments. Most of these changes render the local region with an increased surface accessibility (Fig. 4B). We analysed the change in the relative surface area (RSA) for each characteristic mutation in these lineages. In total,  $\approx 70\%$  of the characteristic mutations in B.1.351 and Delta lineages showed a significant increase in the surface area, and the rest remained unchanged. The P.1 and B.1.526 lineages showed limited increased RSA for 40% and 16.7% of its defining mutations, respectively. Interestingly, the average RSA for the entire RBM across all the key lineages ( $39.05 \text{ \AA}^2$ ) was comparable to WT RBM ( $39.75 \text{ \AA}^2$ ), except for the B.1.526 lineage which displayed a relatively lower average RSA ( $37.44 \text{ \AA}^2$ ) for its RBM region.

In addition, we have analysed the existing cryo-EM structures of spike protein variants, and found a good concordance with our structural analysis. In particular, we have compared the structural models of B.1.1.7 (PDB ID: 7EDF, 7EDG, 7EDH), B.1.351 (PDB ID: 7LYQ), and P.1 (PDB ID: 7M8K). Due to several missing patches harbouring characteristic mutations or unavailable deleted segments, direct quantitative analysis was challenging. However, for the three B.1.1.7 cryo-EM structures, we observed similar side-chain orientation of these substitutions in the structural models generated from this work (Fig. S4). The overall RMSD of our model with B.1.1.7 cryo-EM structures are- PDB ID: 7EDF =  $3.03 \text{ \AA}$ , 7EDG =  $2.75 \text{ \AA}$ , and 7EDH =  $2.70 \text{ \AA}$ . Similar sidechain orientations for the mutated residues were observed for P.1 and B.1.351 cryo-EM structures. Overall, the minimised structural models for VoCs provide a good estimate of substituted structural locations within spike protein.

We further explored additional structural parameters from the COVID-3D resource for characteristic mutations to gain insights into the implications of SARS-COV-2 mutations on the structure (Portelli et al., 2020). COVID-3D provides a missense tolerant score (MTR) for each variant which is a measure of tolerance towards that substitution. Remarkably, these variant patches show a great concordance with MTR scores that reflect how these mutations are tolerated, with an average MTR score of 0.81 and 0.75 for the mutations in the NTD and RBD, respectively. For the characteristic NTD mutations across VoCs (L18F, T19R, T20N, D80A, and T95I), we observed the MTR score of  $\approx 0.738$  suggesting that these mutations show a neutral impact on the protein structure. Further, for the characteristic RBD mutations across VoCs (K417 N/T, L452R, S477N, T478K, E484K, and N501Y), we observed MTR scores between 0.68 and 0.91, suggesting these substitutions to be tolerant.

Next, we investigated the secondary structural features of the regions where these substitutions and deletions occur in these key lineages (Fig. S5). Interestingly, majority of the characteristic mutations (21 out of

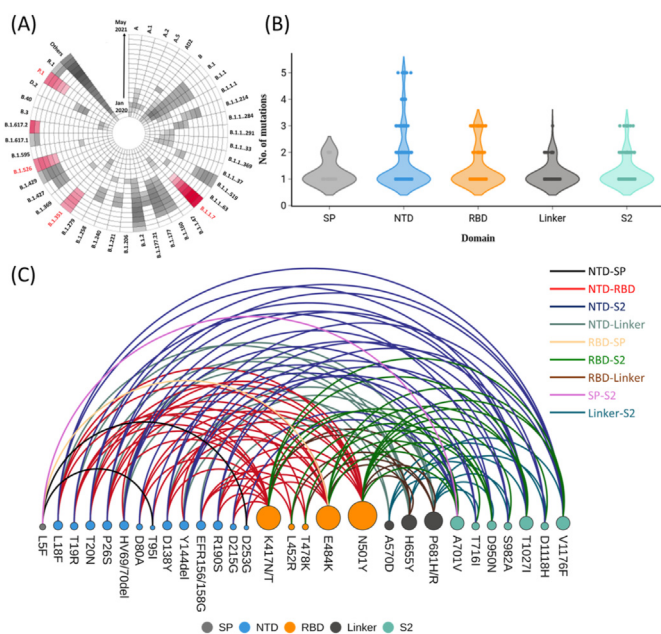


**Fig. 3. Dynamical tracking of genomes reveal spike protein mutational ensemble.** (A) The circular plot shows temporal progression of occurrence of top lineages over a span of 17 months (January 2020–May 2021). The color gradient highlights the prevalence of particular lineage in each month, where the key lineages are highlighted in red color. (B) The violin plot depicts domain-wise distribution of defining mutation present in each lineage where each dot represents a lineage. (C) The arc diagram plots the network of co-occurring mutations between different spike domains, where the size of the node denotes the degree and edges are colored according to the inter-domain connections. (For interpretation of the references to colour in this figure legend, the reader is referred to the web version of this article.)

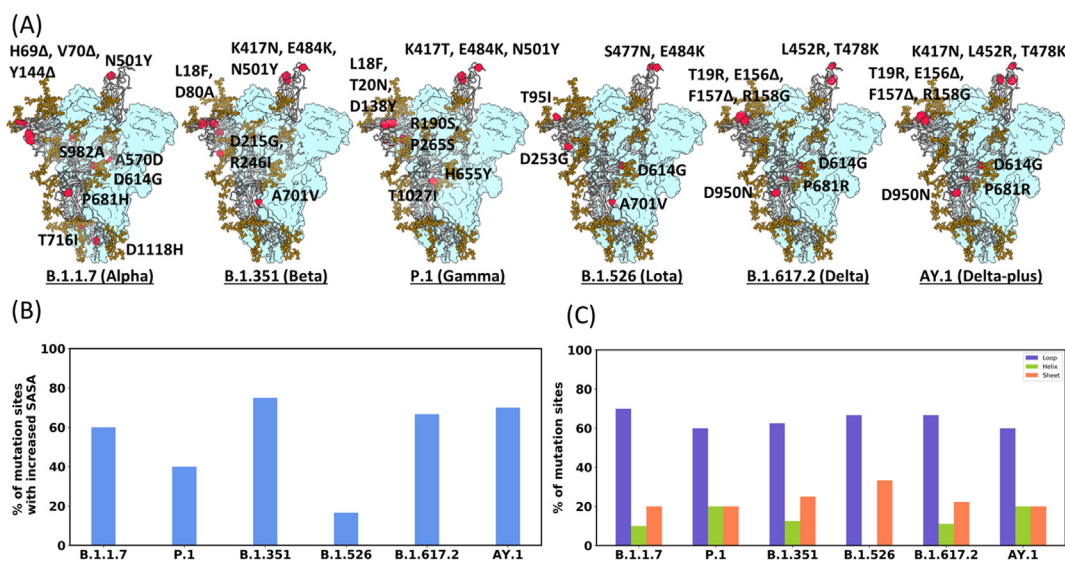


**Fig. 4. Altered relative surface area and presence of the mutations on variable loops.** (A) Structural snapshots of the characteristic mutations in each key lineage are highlighted in red spheres on one of the chains of the spike trimer, with the glycans highlighted in brown. (B) The relative surface area for each mutation site in all variant models was analysed. The bar plot depicts the percentage of the characteristic mutations resulting in an increased surface accessibility as compared to the WT. (C) The grouped bar plot shows the quantitative measure for the secondary structure assessment of each variant and the presence of their respective characteristic mutations on the variable loop region, sheet, and helix of the spike protein. (For interpretation of the references to colour in this figure legend, the reader is referred to the web version of this article.)

35) in these selected key lineages reside within variable loop regions, as can be seen from Fig. 4C. 70% of the characteristic mutations in the B.1.1.7 lineage occur in the loop regions. Similarly, in the B.1.526 and B.1.617.2 lineages, 66.7% of the characteristic mutations are harbored in the loops, whereas in P.1, B.1.351, and AY.1 lineages, the location of these mutation sites quantifies to be 60–62.5%. Further, 12 out of 15 mutations in the NTD and 4 out of 7 mutations in the RBD across all five VOCs and B.1.526 fall in the variable loop region. These findings reveal that mutations are relatively increasing the surface accessibility of mutated loci and loop regions are accruing more mutations.

#### 2.5. Probing local interaction network of spike protein revealed dense hotspots in Delta variant

We were further interested in understanding how combination of amino-acid substitutions may alter overall protein interaction network. By comprehensively analysing the intra-molecular hydrogen bonds, salt-bridges, and hydrophobic contacts in these key lineage structural models, we observed significant variations in non-covalent bond pattern compared to wild-type structure (Fig. 5A; Fig. S6). The number of hydrogen bonds increased by 34.8% in these variants as compared to the WT with 330 unique hydrogen bonds formed. For instance, in B.1.617.2 (Delta variant) four hydrogen bonds upon T19R mutation were found, whereas only one hydrogen bond was observed at this site in the WT protein structure. Whereas, one of the two major deletions in the NTD of B.1.617.2 variant resulted in the loss of 4 hydrogen bonds mediated by E156 in the WT (Fig. S7). Another consecutive substitution, R158G also perturbed the formation of 5 hydrogen bonds in the variant. The RBD of B.1.617.2 harbors two defining mutations (L452R and T478K), out of which L452R substitution enhanced the local hydrogen bond networking by forming 3 bonds as compared to the one in WT (Fig. 5B; Fig. S8). There were 18 salt-bridges in the WT spike which were found to be retained in the VOCs. However, 8 unique salt-bridges were observed in the variants, out of which 2 lie in the NTD, 2 in the RBD, and 4 in the S2 subunit. The number of interactions driven by hydrophobic residues also significantly increased, with 32 novel contacts observed in the VOCs.

Next, to examine the impact of these mutations on the protein structure, we calculated domain-wise residue interaction network (RIN)

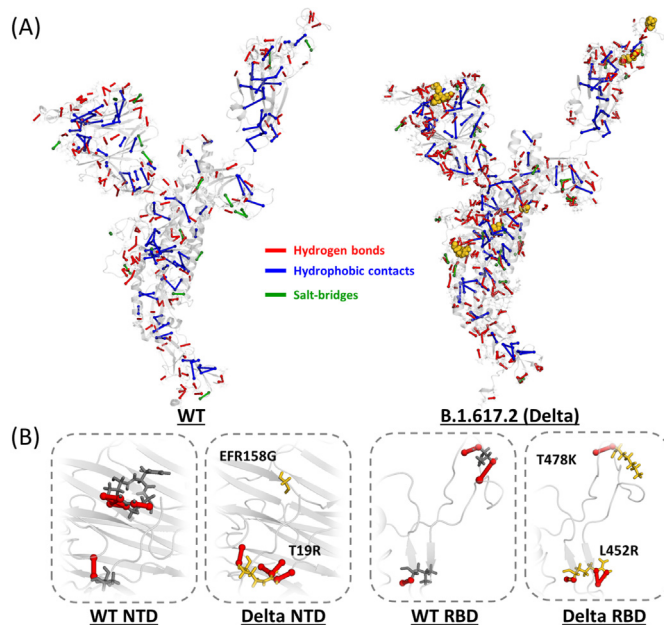


**Fig. 5. Intra-protein interaction network of WT vs B.1.617.2 spike.** (A) Comparative global intra-molecular network for WT and Delta spike protein, where unique hydrogen bonds are marked in red on one of the chains of spike trimer. The total number of salt bridges and hydrophobic contacts are highlighted in green and blue, respectively and the mutations of B.1.617.2 are marked in yellow. (B) The zoomed-in panels display the comparison between local hydrogen bond network around the characteristic mutations for which the side chains are shown in stick representation in the NTD and RBD of the WT and Delta variant. (For interpretation of the references to colour in this figure legend, the reader is referred to the web version of this article.)

in wild-type and six key spike variants, namely- B.1.1.7, B.1.351, P.1, B.1.526, B.1.617.2, and AY.1. In these networks, residues are represented as nodes and contacts between them are edges. Comparative analysis of networks of VOCs with wild-type revealed perturbations in local contacts

and there is an overall increase in the total number of intra-protein contacts in these key lineages. Remarkably, the intra-molecular RBD contacts increased significantly with 660 additional contacts or edges and 70% of the residues displayed a degree  $>10$ . In B.1.1.7 lineage, there is one critical mutation in the RBM namely- N501Y, which has been reported previously to enhance the interaction with the hACE2 (Zahradnik et al., 2021; Zhu et al., 2021). Hence, we analysed the inter-protein interaction network of the binding interface between the RBD and hACE2 (Fig. S9). Structural analysis of the WT and B.1.1.7 variant bound to hACE2 revealed the formation of a high number of contacts after N501Y substitution. Similarly, P.1 and B.1.351 lineages have three key mutations in the RBM, namely- K417 T/N, E484K, and N501Y. For K417T in B.1.351 lineage, no significant alterations were observed. Whereas, most of the RBM residues in AY.1 variant displayed enhanced contacts (Fig. S10). All the potent NTD targeting antibodies recognize the 'NTD supersite', consisting of the N1, N3, and N5 loop (Lok, 2021). In the wild-type structure, NTD displayed a total of 2843 local contacts with 52% of the NTD residues having a degree of  $>10$ . The higher degree residues comprised 8 out of the 17 characteristic mutation sites in NTD across the key lineages (T19, H69, Y144, E156, R158, R190, R246 & D253). Although B.1.1.7 intra-NTD network is supported by 233 residues with higher degree contacts, three deletions in the N2 loop of the NTD (H69del, V70del & Y144del) greatly perturb the local interaction network which was observed to mediate around 10, 9, 15 local contacts each in the WT spike, respectively. Similar alterations were observed around the furin cleavage site with 44% more number of contacts within protein residues.

We speculate that these intramolecular changes may directly impact increased virulence or enhanced immune escape features of VOCs. For instance, the deletions present within NTD in multiple lineages (HV69/70del, Y144del, E156-F157del) are predicted to vary the conformation of an exposed NTD loop. This particular loop has been associated with increased infectivity (McCallum et al., 2021). Also, the changes within NTD occur on prominent mAbs recognition sites (Liu et al., 2020). In the mutated model of B.1.617.2, R19 residue is surface accessible while in wild-type the T19, was relatively buried. Across RBD, some mutations clearly confer immune escape (Barton et al., 2021). The T478K is present directly on the RBM, and the long side chain of K478 might impact the neighbouring ACE2 residues in contact with the RBD residues. We observed formation of new contacts around the mutation site, implying stronger binding to ACE2. The presence of a furin cleavage site is important for infectivity and virulence of SARS-CoV-2 and mutation near this region has been reported to lead to conformational changes that impact pre-fusion stable structure (Gobeil et al., 2020; Wrobel et al., 2020). These findings suggest that combinations of mutations present in VoCs lineages perturb the local interactions other than exact point of substitution and we further speculate that these rewired contacts may influence functionally important regions.

## 2.6. Molecular dynamics simulations of full-length D614G spike showed structurally flexible regions

Collective internal motions in proteins are linked with the full-length spike structural model of wild-type and one mutant structure of spike

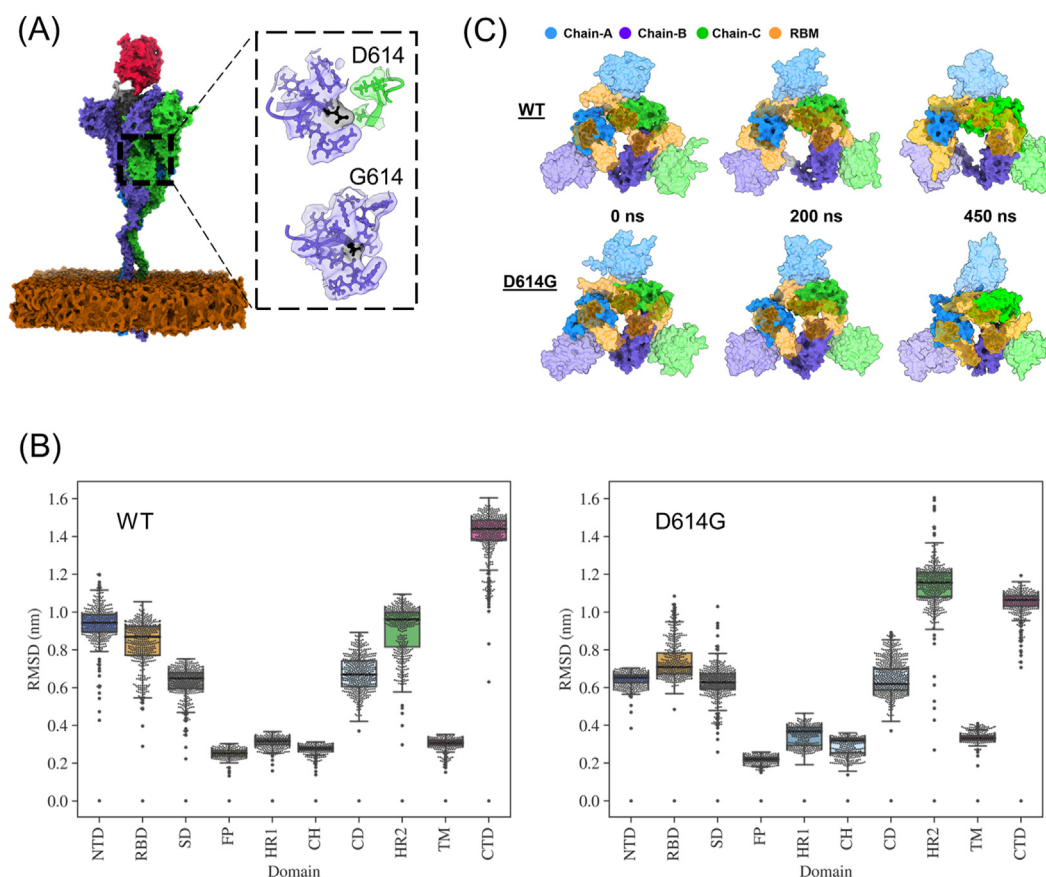


**Fig. 6. Dynamics of the wild-type and D614G mutant spike.** (A) Full-length 1-RBD-up spike model in the POPC membrane-bound to hACE2 is depicted. The zoomed-in image highlights the residues within 5 Å of the 614th residue in WT and mutant, where 614 is highlighted in black color. (B) Box plot showing the domain-wise distribution of RMSD in WT & mutant trajectories in the left and right panel, respectively. (C) Snapshots showing the dynamics of RBM with respect to the RBD and NTD in WT & D614G mutant spike protein as a function of time. The structures are shown in surface representation with chains A, B, and C colored in blue, purple, and green, respectively while brown shows the RBM motif. (For interpretation of the references to colour in this figure legend, the reader is referred to the web version of this article.)



protein in an open state. From here the 1-RBD-up spike structures bound to hACE2 were inserted into the membrane and each system was simulated for 450 ns each (Fig. 6A). In comparison to the starting structure, root mean square deviations were plotted for each domain (Fig. 6B). Our analysis revealed increased stability of the D614G protein ( $0.89 \pm 0.007$  nm) as compared to the WT spike system (Fig. S11). Interestingly, a relative decrease in the deviation of mutant NTD ( $0.63 \pm 0.002$  nm) and RBD regions ( $0.74 \pm 0.005$  nm) was found, as shown in Fig. 6B. In addition to RBD and NTD, high flexibility was found in the HR2 and CTD which have been linked to post-fusion event (Huang et al., 2020; Turoňová et al., 2020). Followed by the RBD, the SD1 (542–591 a.a.) and SD2 (592–681 a.a.) regions showed a similar trend in both the WT and D614G systems with an average RMSD of  $0.61 \pm 0.003$  nm. Fig. 6C shows the representative snapshots highlighting dynamical changes within the NTD and RBD regions at different time frames. Specifically, the RBM in D614G ( $0.72 \pm 0.002$  nm) is observed to be relatively stable as compared to that of the WT system ( $1.00 \pm 0.009$  nm).

Interestingly, each of the spike protein monomers is inter-twinned in such a fashion that it orients the RBD closer to the next chain NTD. We analysed the correlation between the RBD and NTD of each chain and our analyses revealed that the distances between these domains are higher in the wild-type (6.20 nm and 6.48 nm). In the D614G trajectory, it corresponded to a relatively compact state with significantly less distance between the NTD and RBD (5.97 nm and 5.82 nm, respectively) as shown in Fig. S12. This results in a compact conformation of the D614G and more importantly results in higher proximity with the hACE2 structure. Mapping of the flexibility parameter, root mean square fluctuations (RMSF) of both domains revealed significant stability in mutant structures (Fig. S13). In wild-type, we observed distinct patches within the NTD (142–152, 180–184, and 248–257) and RBD (474–490, 496 to 503) that are highly mobile. The simulations were performed under limiting conditions, especially the heterogeneous membrane lipids that were not considered. However, we obtained dynamics of full-length spike that allowed us to further map mutations onto the dynamical regions. Approximately, 43.6% and 12.67% of the total mutations of the spike are present in the NTD and RBD domain, respectively.

Various surface epitopes have been proposed to be present on the spike structures. Three distinct regions, namely, N-terminus (residues 14–20), a supersite  $\beta$ -hairpin (residues 140–158), and a supersite loop (residues 245–264) constitute epitopes within the NTD region (McCallum et al., 2021). Similarly, the RBD epitopes are characterised as the ridge (residues 455–456, 471–491), loop (residues 443–453, 494–502), and core (residues 365–373, 382–387) (Greaney et al., 2021). We have mapped these prevalent mutations on these known epitopes of NTD and RBD on full-length spike structure (Fig. S14). Out of 22 mutations in the NTD region, nine mutations are located in the NTD epitope region. Specifically, L18F, T19R, and T20N are present in the N-terminus epitope, whereas G142D, W152 R/L/C, M153T, and F157 are present in the supersite  $\beta$ -hairpin epitope. D253G and A262S are present in the supersite loop epitope of NTD. Interestingly, five out of eight mutations of RBD are present in the epitope region, where L452R and N501Y substitutions map to the RBD-loop epitope and S477N, T478K, and E484K are harboured in the RBD-ridge epitope.

We further characterised these epitope regions with respect to the flexibility or rigidity of the region. For this, we integrated our structural knowledge of these epitopes with the understanding of the dynamic regions of spike protein, primarily NTD and RBD from our MD simulations using RMSF as the parameter. All three NTD epitopes map to the highly fluctuating regions. Out of all the RBD epitopes, the RBD-ridge epitope is present in the higher flexible region, whereas the RBD-loop epitope is present in the moderately flexible region. While the RBD-core epitope is present at a very less flexible region of RBD. We speculate that these flexible regions evolve faster and hence play a key role in protein function.

### 3. Discussion and conclusions

There are several driving forces for and against the selection determining the fitness advantage. The timely tracking of the sequencing of SARS-CoV-2 genomes in parallel with a large number of structural data has enabled several quick biological discoveries (Neher et al., 2020). During the ongoing pandemic, the genomes served as quick indicator maps and provided real-time tracking of key mutations (Rambaut et al., 2020; Faria et al., 2021). Especially, mutations on the SARS-CoV-2 spike protein are of substantial interest as they directly induce antibody response. Several vaccine candidates are also focused on spike protein (Martínez-Flores et al., 2021). Therefore, comprehensive efforts are required to decompose structural factors responsible for altered interactions in spike variants.

Here, we dynamically tracked genomic variations of SARS-CoV-2 spike protein submitted in GISAID over a span of 17 months which enabled a pan-spike mutational analysis that revealed more than 2500 mutations on the protein. We found precise mutational hotspots that are accruing more mutations and emphasize that there exists selective pressure on these stretches. Apart from well-characterised RBD region, several loops of NTD showed hypervariable regions. In addition, SARS-CoV-2 lineages mutations exhibit NTD mutations co-occurring with RBD, Linker, and S2 domain, indicating coaxial framework of mutations. Further structure-based analysis of VOCs revealed that mutated side chains appear on surfaces and loops. Dense local networks around functionally important regions were significantly perturbed in VOCs. A caveat of the present structural analysis of VOCs is estimation of structural properties based on minimised structural snapshots. Our simulations of the D614G spike variant bound to ACE2 further elaborates on dynamical features with increased compactness in the NTD-RBD region.

Previous experimental studies have also revealed amino acid properties that directly impact spike protein function by altering infectivity, transmissibility, or antigenicity (Zhang et al., 2020; Harvey et al., 2021; Volz et al., 2021; Hu et al., 2020). Barton et al. studied the effect of five prevalent RBD mutations (K417N, K417T, N501Y, E484K, and S477N) on RBD-ACE2 interaction and suggested that the N501Y, E484K, and S477N mutations showed increased affinity towards ACE2 binding as compared to the wild type which might enhance transmission. However, the amino acid substitution of lysine at 417 position to either asparagine or threonine facilitates immune escape (Barton et al., 2021). Several studies have contributed to the understanding of how spike mutations affect immunogenicity, especially mutations within RBD (Weisblum et al., 2020; Wang et al., 2021b; Liu et al., 2021). Further, deep mutational scanning of SARS-CoV-2 RBD has revealed that most of the prevalent RBD mutations are tolerant towards protein folding and ACE2 binding (Starr et al., 2020). Thus, the possibility of immune escape still exists under strong selection pressure. In a comparative study between single-antibody escape and cocktail therapy, the latter was observed to provide a powerful way to minimize mutational escape by SARS-CoV-2 (Baum et al., 2020). Our studies also point that the mutated structural model from combined set of characteristic mutations in VOCs is greatly altered, and thus antibodies targeted to topologically distinct regions may be beneficial.

Recently, multiple cryo-EM structures of spike protein variants have also been determined (Wang et al., 2021a; Gobeil et al., 2021; Yang et al., 2021). The D614G spike has revealed varied interactions within protomer that induce conformational changes within the S1 subunit (Zhang et al., 2021; Yan et al., 2021). These changes, largely based on closed conformations, propose that mutant G614 is stable and that it increases the number of spikes that can facilitate infection (Yurkovetskiy et al., 2020). We have also compared our data with cryo-EM derived VoCs structural data. Interestingly, minimised structural model and experimental structures show similar side chain orientations that also correspond to higher accessibility. Interestingly, prevalent amino acid

substitutions such as A222V, Y453F have also been linked with structural perturbations or ACE2 binding (Hodcroft et al., 2021; Starr et al., 2020). However, these changes are not participating as a defining mutation in any VOCs.

Several computational approaches have been applied to study spike variants (Celik et al., 2021; Antony and Vijayan, 2021). For instance, early during the pandemic, the COVID-3D online resource provided extensive spatial maps of SARS-CoV-2 mutations and an overall missense tolerance score for each mutation (Portelli et al., 2020). Another report during early pandemic listed the hypervariable genomic hotspots within entire SARS-CoV-2 (Wen et al., 2020). Mutations hotspots have also been characterised using Shannon Entropy and K-means clustering that reveal positions that are most susceptible to mutations (Mullick et al., 2021).

The focus of the present study was to provide structural view on extensive genomics variations within spike protein for a period of 17 months and how these mutations alter structural properties. Additionally, a large number of previous computational studies have focussed on extensive dynamics of spike protein and its variants. Multiple all-atom molecular dynamics simulations of spike protein revealed essential structural role of N-glycan at sites N165 and N234 (Casalino et al., 2020). The critical glycan positions were found to modulate conformational dynamics of RBD which is responsible for ACE2 binding. In a massive effort by Folding@home distributed computing project, spike protein simulations predicted complete opening of spike protein and substantial conformational heterogeneity in the open state (Zimmerman et al., 2021). Further, over 130  $\mu$ s of weighted ensemble simulations of the fully glycosylated spike protein provided kinetically unbiased RBD opening pathways and revealed a gating role for the N-glycan at position N343. In another study, a total of 20  $\mu$ s MD simulation trajectory of both wild type and D614G mutant provided mechanistic details of the increased occupancy of open state in G614 form (Mansbach et al., 2021). Utilising a different approach of normal mode analysis, Teruel et al., calculated transition probabilities between the open and closed states, and proposed an increase in open state occupancy for more infectious D614G mutant and a similar effect was proposed on glycine residues (404, 416, 504, and 252) as well as residues K417, D467, and critical N501Y mutation site (Teruel et al., 2021). In another interesting approach, neural network model based on molecular dynamics simulations accurately mapped simulated binding energies to experimental changes in the binding strength upon spike protein mutations (Chen et al., 2021).

In our earlier detailed work on Delta variant surge in Delhi, we speculated that three locations: RBD, NTD, and furin cleavage site are collectively evolving for higher transmission (Dhar et al., 2021). Clearly, much remains to be learned, in terms of which mutational combinations and how their functional interactions (if any) change the biological function of the virus. Either way, analysis of high-throughput data and association with clinical markers must go hand in hand.

## 4. Materials and methods

### 4.1. Genome data acquisition and analysis

In total, 1,624,465 spike protein sequences of SARS-CoV-2 genome were downloaded from the GISAID database submitted till 31 May 2021 (Shu and McCauley, 2017). The low-quality sequences were removed and the genomes having high coverage greater than 90% were considered. 527,988 genomes passed the filtering criteria for specific seven geographies and were taken for further analysis. The additional details associated with these genomes including geography and date of submission was also considered for this study. Specifically, we selected 7 geographic regions, China (1,456), India (16,768), Brazil (3,936), South Africa (3,691), Australia (13,819), USA (287,843), and UK (200,475); constituting 62.24% of the total genomes. In addition, we also included 8477 Indian genomes sequenced by NCDC, Delhi submitted to GISAID later to 31 May 2021. Any sequences without proper submission details were dropped

out. The variant annotation was done using CoVsurver enabled by GISAID in GISAID's EpiCoV database and Wuhan 2019-nCoV genome (GISAID Accession ID: EPI\_ISL\_402124) was used as the reference genome for mutational analysis (Okada et al., 2020). The quality check was performed and all the abrupt genomic sequences with more than 20 mutations per sample were removed. We also characterised month-wise genomic information to capture the time progression of spike variants. To remove the noise, we analysed mutations present in at least 1% of the total samples in selected time duration. We assigned lineage information for each sequence using Phylogenetic Assignment of Named Global Outbreak Lineages (PANGOLIN) resource (O'Toole et al., 2021). For analysing the inter-domain co-occurring combinations, we extracted the defining mutations for the six major lineages.

### 4.2. Generation of hACE2-bound 1-RBD-up spike conformation

For extensive characterisation of spike protein using molecular dynamics simulations, we generated the full-length model of spike consisting of 1273 residues in an open conformation. The cryo-EM structure of the spike RBD-up state (PDB ID 6VSB) was taken as the template. In addition, the HR2 region was modeled using the NMR structure of the HR2 domain from SARS-CoV (PDB ID 2FXP) while that of the TM region was generated using the NMR structure of HIV-1 Env polyprotein (PDB ID 5JYN) having a homology of 100% and 29% with the spike protein, respectively. The PDB ID 5JYN was taken as it was the only template available for the TM region at the time of model generation. The missing residues in the structure were modeled as loops except for residues 1148–1161 which were restraint to form an alpha-helix. The structural model was generated in 3 segments: 14–1147, 1148–1213, and 1214–1273 and were joined together using the standard peptide-bond criteria in Chimera (Pettersen et al., 2004a). To obtain a complete atomistic model of hACE2, we took the X-ray structure of human ACE2 bound to the RBD domain (PDB ID: 6M0J) as template. The D614G mutation was then introduced in all three chains of the model in UCSF Chimera. The full-length spike model of 1-RBD-up state bound to hACE2 was oriented in the membrane containing 2068 POPC lipids. The membrane was generated using VMD and the spike structure was embedded in the membrane using InflateGRO2 (Humphrey et al., 1996; Kandt et al., 2007). The transmembrane residues (1214–1273) were positioned in the membrane by translating the protein along the Z-axis.

### 4.3. Generation of wild-type and variant glycosylated spike protein models

The protein structure PDB ID 7A94 was taken as a reference structure to generate wild-type spike model. This structure is a higher resolution structure available for open bound conformation of spike consisting of 1146 residues (Benton et al., 2020). The complex structure depicts the 1-RBD-up conformation in spike protein, with the limited missing regions [71–75, 625–632, 677–688, 828–852, and 941–943] modeled using Modeler. The hACE2 structure in the template also had six residues missing patch that were added by taking PDB ID 1R42 as a reference. The complete 1146 spike-hACE2 structural model was used as a template to create variant models using Dunbrack 2010 backbone-dependent rotamer library in Chimera (Shapovalov and Dunbrack Jr, 2011). Further processing of steps was done using Gromacs toolkit. The deletions for B.1.1.7, B.1.617.2 and AY.1 spike were introduced and adjacent residues were joined by introducing the peptide bond. The mutated structural models were subjected to minimization in vacuum for extensive sidechain minimization. The final step involved addition of glycosylation using the Glycan Reader & Modeler of Charmm-GUI (Jo et al., 2011). The detailed information of the site and type of glycosylation for each chain of spike was taken from Casalino et al. (2020) study (Casalino et al., 2020). All the glycosylated structural models are available on the github link of this paper.



#### 4.4. Analysis of structural properties

The relative solvent-accessible surface area for each residue in spike WT as well as the variants was calculated by Naccess (Hubbard and Thornton, 1993) and the secondary structure assessment was performed using STRIDE (Heinig and Frishman, 2004). We utilized network approach to study the alterations in the local contact network around the characteristic mutation sites. To obtain hydrophobic contacts, salt bridges and hydrogen bonding pattern for each of the structural model, the intra-protein interactions analysis has been carried out by using Pyinteraph and the interaction plotter (pymol plugin) was used to map the interactions identified by Pyinteraph on the 3D-spike structure (Tiberti et al., 2014). For the contact based intra-protein network, we took a cut-off of 3.5 Å to define the existence of a hydrogen bond between sidechain of residues and mainchain-sidechain residue atoms. For salt bridges, the charged residues were considered interacting if at least one pair of atoms is at a distance within the cut-off.

In addition, we also analysed inter-protein contacts between hACE2 and spike RBD region. We performed the network construction for our glycosylated spike structural models of WT and variants to capture the changes occurring within the binding interface. For this we considered the interface residues of RBD (400–508 a.a) and hACE2 (19–100 a.a, 300–360 a.a) and the co-ordinates for hACE2 were saved from the PDB ID 7A94. RINalyzer plugin in Cytoscape 3.8.2 was used to construct the networks (Demchak et al., 2014; Doncheva et al., 2011). The nodes represent the residues and the interactions between residues are edges of the network. A cut-off distance of 4 Å was used to define a contact.

#### 4.5. Molecular dynamics simulations

The full-length hACE2-bound 1-RBD-up complex structure in membrane was placed in a rectangular box large enough to contain the protein and the membrane. Na<sup>+</sup> ions were added to neutralize and TIP3P water representation was used to solvate the system (Mark and Nilsson, 2001). The simulations were carried out using GROMACS version 2018.3 by employing the CHARMM36 all-atom force field (Abraham et al., 2015). Periodic boundary conditions were used and 1.2 nm was set as real space cut-off distance. Particle Mesh Ewald (PME) summation using the grid spacing of 0.16 nm was used in combination with a fourth-order cubic interpolation to deduce the forces and potential in-between grid points (Darden et al., 1993). The Van der Waals cut-off was set to 1.2 nm. A 2 fs time step for numerical integration of the equations of motion was used and the coordinates were saved at every 100 ps. The initial systems were subjected to energy minimization using the steepest descent method. Temperature and pressure were maintained at 310 K and 1 bar using Nose-Hoover thermostat and Parrinello-Rahman barostat, respectively (Bussi et al., 2007; Parrinello and Rahman, 1981). Simulations of both wild-type and D614G systems were carried out for 450 ns each. All the molecular images were rendered using UCSF Chimera and ChimeraX (Pettersen et al., 2004b, 2021), VMD, (Humphrey et al., 1996) and PyMOL (Schrödinger, LLC, 2015). The graphs and plots were generated using Python libraries.

#### Authors contribution

All authors contributed to the study conception and design. SF and SR collected and analysed the structural and genomic data. MD simulation study and structural analysis were also performed by SR and SF. NB and DG contributed to the additional analyses and interpretation of the data. AP and MM analysed the geographical distribution of mutations. LT supervised the study and helped in the interpretation of the results. SF, SR, and LT wrote the manuscript.

#### Data availability

The data files related to the genomic analyses, structural models, and

MD simulation trajectories have been made available at [https://github.com/CSB-Thukral-Lab/spike\\_genomic\\_and\\_structural\\_work](https://github.com/CSB-Thukral-Lab/spike_genomic_and_structural_work).

#### CRedit authorship contribution statement

**Saman Fatih:** Conceptualization, Methodology, Data curation, Writing – original draft, preparation. **Surabhi Rathore:** Conceptualization, Methodology, Data curation, Writing – original draft, preparation. **Ankit K. Pathak:** Visualization, Formal analysis. **Deepanshi Gahlot:** Visualization, Formal analysis. **Mitali Mukerji:** Formal analysis, Investigation. **Nidhi Jatana:** Visualization, Formal analysis. **Lipi Thukral:** Conceptualization, Writing – original draft, Writing – review & editing, Supervision.

#### Declaration of competing interest

The authors declare that they have no known competing financial interests or personal relationships that could have appeared to influence the work reported in this paper.

#### Acknowledgements

This work was supported by funding from CSIR and the Department of Science and Technology (DST). S.F. is supported by DST Early Career Award, S.R. by DST-Inspire fellowship, D.G. by CSIR-NET fellowship, and N.J. by DST-SERB fellowship. We acknowledge the support from CSIR-IGIB for infrastructure and CSIR-4PI for supercomputing facilities.

#### Appendix A. Supplementary data

Supplementary data to this article can be found online at <https://doi.org/10.1016/j.crstbi.2021.11.002>.

#### References

- Abraham, M.J., Murtola, T., Schulz, R., Páll, S., Smith, J.C., Hess, B., Lindahl, E., 2015. GROMACS: high performance molecular simulations through multi-level parallelism from laptops to supercomputers. *SoftwareX* 1–2, 19–25. <https://doi.org/10.1016/j.softx.2015.06.001>.
- Amanat, F., Thapa, M., Lei, T., Ahmed, S.M.S., Adelsberg, D.C., Carreño, J.M., Strohmeier, S., Schmitz, A.J., Zafar, S., Zhou, J.Q., et al., 2021. Sars-cov-2 mrna vaccination induces functionally diverse antibodies to ntd, rbd, and s2. *Cell* 184, 3936–3948.
- Andersen, K.G., Rambaut, A., Lipkin, W.I., Holmes, E.C., Garry, R.F., 2020. The proximal origin of sars-cov-2. *Nat. Med.* 26, 450–452.
- Annavaiahala, M.K., Mohri, H., Wang, P., Nair, M., Zucker, J.E., Sheng, Z., Gomez-Simmonds, A., Kelley, A.L., Tagliavia, M., Huang, Y., et al., 2021. A Novel and Expanding Sars-Cov-2 Variant, B. 1.526, Identified in New York. *medRxiv*.
- Antony, P., Vijayan, R., 2021. Role of sars-cov-2 and ace2 variations in covid-19. *Biomed. J.* June 2021, 235–244. <https://doi.org/10.1016/j.bj.2021.04.006>.
- Barnes, C.O., Jette, C.A., Abernathy, M.E., Dam, K.M.A., Esswein, S.R., Gristick, H.B., Malyutin, A.G., Sharaf, N.G., Huey-Tubman, K.E., Lee, Y.E., Robbiani, D.F., Nussenzweig, M.C., West, A.P., Bjorkman, P.J., 2020. SARS-CoV-2 neutralizing antibody structures inform therapeutic strategies. *Nature* 588, 682–687. <https://doi.org/10.1038/s41586-020-2852-1>.
- Barton, M.I., MacGowan, S.A., Kutuzov, M.A., Dushek, O., Barton, G.J., van der Merwe, P.A., 2021. Effects of common mutations in the sars-cov-2 spike rbd and its ligand the human ace2 receptor on binding affinity and kinetics. *Elife* 10, e70658.
- Baum, A., Fulton, B.O., Wloga, E., Copin, R., Pascal, K.E., Russo, V., Giordano, S., Lanza, K., Negron, N., Ni, M., et al., 2020. Antibody cocktail to sars-cov-2 spike protein prevents rapid mutational escape seen with individual antibodies. *Science* 369, 1014–1018.
- Benton, D.J., Wrobel, A.G., Xu, P., Roustan, C., Martin, S.R., Rosenthal, P.B., Skehel, J.J., Gamblin, S.J., 2020. Receptor binding and priming of the spike protein of SARS-CoV-2 for membrane fusion. *Nature* 588, 327–330. <https://doi.org/10.1038/s41586-020-2772-0>.
- Bussi, G., Donadio, D., Parrinello, M., 2007. Canonical sampling through velocity rescaling. *J. Chem. Phys.* 126, 014101. <https://doi.org/10.1063/1.2408420>.
- Casalino, L., Gaieb, Z., Goldsmith, J.A., Hjorth, C.K., Dommer, A.C., Harbison, A.M., Fogarty, C.A., Barros, E.P., Taylor, B.C., McLellan, J.S., Fadda, E., Amaro, R.E., 2020. Beyond shielding: the roles of glycans in the SARS-CoV-2 spike protein. *ACS Cent. Sci.* 6, 1722–1734. <https://doi.org/10.1021/acscentsci.0c01056>.
- Celik, I., Yadav, R., Duzgun, Z., Albogami, S., El-Shehawi, A.M., Idroes, R., Tallei, T.E., Emran, T.B., et al., 2021. Interactions of the receptor binding domain of sars-cov-2

- variants with hacc2: insights from molecular docking analysis and molecular dynamic simulation. *Biology* 10, 880.
- Chen, C., Boorla, V.S., Banerjee, D., Chowdhury, R., Cavener, V.S., Nissly, R.H., Gontu, A., Boyle, N.R., Vandegriff, K., Nair, M.S., et al., 2021. Computational prediction of the effect of amino acid changes on the binding affinity between sars-cov-2 spike rbd and human ace2. *Proc. Natl. Acad. Sci. Unit. States Am.* 118.
- Chen, X., Li, R., Pan, Z., Qian, C., Yang, Y., You, R., Zhao, J., Liu, P., Gao, L., Li, Z., Huang, Q., Xu, L., Tang, J., Tian, Q., Yao, W., Hu, L., Yan, X., Zhou, X., Wu, Y., Deng, K., Zhang, Z., Qian, Z., Chen, Y., Ye, L., 2020. Human monoclonal antibodies block the binding of SARS-CoV-2 spike protein to angiotensin converting enzyme 2 receptor. *Cell. Mol. Immunol.* 17, 647–649. <https://doi.org/10.1038/s41423-020-0426-7>.
- Chi, X., Yan, R., Zhang, J., Zhang, G., Zhang, Y., Hao, M., Zhang, Z., Fan, P., Dong, Y., Yang, Y., Chen, Z., Guo, Y., Zhang, J., Li, Y., Song, X., Chen, Y., Xia, L., Fu, L., Hou, L., Xu, J., Yu, C., Li, J., Zhou, Q., Chen, W., 2020. A neutralizing human antibody binds to the n-terminal domain of the spike protein of SARS-CoV-2. *Science* 369, 650–655. <https://doi.org/10.1126/science.abc6952>.
- Dai, L., Gao, G.F., 2021. Viral targets for vaccines against covid-19. *Nat. Rev. Immunol.* 21, 73–82.
- Darden, T., York, D., Pedersen, L., 1993. Particle mesh ewald: AnN-log(n) method for ewald sums in large systems. *J. Chem. Phys.* 98, 10089–10092. <https://doi.org/10.1063/1.464397>.
- Demchak, B., Hull, T., Reich, M., Liefeld, T., Smoot, M., Ideker, T., Mesirov, J.P., 2014. Cytoscape: the network visualization tool for genomespace workflows. *F1000Research* 3.
- Dhar, M.S., Marwal, R., Radhakrishnan, V., Ponnusamy, K., Jolly, B., Bhojar, R.C., Fathi, S., Datta, M., Singh, P., Sharma, U., Ujjainia, R., Naushin, S., Bhatena, N., Divakar, M.K., Sardana, V., Singh, M.K., Imran, M., Senthivel, V., Maurya, R., Jha, N., Mehta, P., Rophina, M., Arvindan, V., Chaudhary, U., Thukral, L., Pandey, R., Dash, D., Faruq, M., Lall, H., Gogia, H., Madan, P., Kulkarni, S., Chauhan, H., Sengupta, S., Kabra, S., (INSACOG), T.I.S.C. G.C., Singh, S.K., Agrawal, A., Rakshit, P., 2021. Genomic Characterization and Epidemiology of an Emerging Sars-Cov-2 Variant in Delhi, India. <https://doi.org/10.1101/2021.06.02.21258076> medRxiv.
- Doncheva, N.T., Klein, K., Domingues, F.S., Albrecht, M., 2011. Analyzing and visualizing residue networks of protein structures. *Trends Biochem. Sci.* 36, 179–182.
- Faria, N.R., Mellan, T.A., Whittaker, C., Claro, I.M., Candido, D.d.S., Mishra, S., Crispin, M.A.E., Sales, F.C.S., Hawrylyuk, I., McCrone, J.T., Hulsmit, R.J.G., Franco, L.A.M., Ramundo, M.S., de Jesus, J.G., Andrade, P.S., Coletti, T.M., Ferreira, G.M., Silva, C.A.M., Manuli, E.R., Pereira, R.H.M., Peixoto, P.S., Kraemer, M.U.G., Gaburo, N., Camilo, C.d.C., Hoeltgebaum, H., Souza, W.M., Rocha, E.C., de Souza, L.M., de Pinho, M.C., Araujo, L.J.T., Malta, F.S.V., de Lima, A.B., Silva, J.d.P., Zauli, D.A.G., Ferreira, A.C.d.S., Schnekenberg, R.P., Laydon, D.J., Walker, P.G.T., Schlüter, H.M., dos Santos, A.L.P., Vidal, M.S., Del Caro, V.S., Filho, R.M.F., dos Santos, H.M., Aguiar, R.S., Proença-Modena, J.L., Nelson, B., Hay, J.A., Monon, M., Miscouridou, X., Coupland, H., Sonabend, R., Vollmer, M., Gandy, A., Prete, C.A., Nascimento, V.H., Suchard, M.A., Bowden, T.A., Pond, S.L.K., Wu, C.H., Ratmann, O., Ferguson, N.M., Dye, C., Loman, N.J., Lemey, P., Rambaut, A., Fraiji, N.A., Carvalho, M.d.P.S.S., Pybus, O.G., Flaxman, S., Bhatt, S., Sabino, E.C., 2021. Genomics and epidemiology of the p.1 sars-cov-2 lineage in manaus, Brazil. *Science* 372, 815–821. <https://doi.org/10.1126/science.abh2644>.
- Gobeil, S., Janowska, K., McDowell, S., Mansouri, K., Parks, R., Manne, K., Stalls, V., Kopp, M., Henderson, R., Edwards, R.J., et al., 2020. D614g Mutation Alters Sars-Cov-2 Spike Conformational Dynamics and Protease Cleavage Susceptibility at the S1/s2 Junction bioRxiv.
- Gobeil, S., Janowska, K., McDowell, S., Mansouri, K., Parks, R., Stalls, V., Kopp, M.F., Manne, K., Saunders, K.O., Edwards, R.J., et al., 2021. Effect of Natural Mutations of Sars-Cov-2 on Spike Structure, Conformation and Antigenicity bioRxiv.
- Graham, C., Seow, J., Huettner, I., Khan, H., Koughou, N., Acors, S., Winstone, H., Pickering, S., Galao, R.P., Lista, M.J., et al., 2021. Impact of the B.1.1.7 Variant on Neutralizing Monoclonal Antibodies Recognizing Diverse Epitopes on Sars-Cov-2 Spike bioRxiv.
- Greaney, A.J., Loes, A.N., Crawford, K.H., Starr, T.N., Malone, K.D., Chu, H.Y., Bloom, J.D., 2021. Comprehensive mapping of mutations in the sars-cov-2 receptor-binding domain that affect recognition by polyclonal human plasma antibodies. *Cell Host Microbe* 29, 463–476.
- Groves, D.C., Rowland-Jones, S.L., Angyal, A., 2021. The d614g mutations in the sars-cov-2 spike protein: implications for viral infectivity, disease severity and vaccine design. *Biochem. Biophys. Res. Commun.* 538, 104–107.
- Harvey, W.T., Carabelli, A.M., Jackson, B., Gupta, R.K., Thomson, E.C., Harrison, E.M., Ludden, C., Reeve, R., Rambaut, A., Peacock, S.J., et al., 2021. Sars-cov-2 variants, spike mutations and immune escape. *Nat. Rev. Microbiol.* 19, 409–424.
- Heinig, M., Frishman, D., 2004. Stride: a web server for secondary structure assignment from known atomic coordinates of proteins. *Nucleic Acids Res.* 32, W500–W502.
- Hodcroft, E.B., Zuber, M., Nadeau, S., Vaughan, T.G., Crawford, K.H., Althaus, C.L., Reichmuth, M.L., Bowen, J.E., Walls, A.C., Corti, D., et al., 2021. Spread of a sars-cov-2 variant through europe in the summer of 2020. *Nature* 595, 707–712.
- Hoffmann, M., Kleine-Weber, H., Pöhlmann, S., 2020a. A multibasic cleavage site in the spike protein of sars-cov-2 is essential for infection of human lung cells. *Mol. Cell* 78, 779–784.
- Hoffmann, M., Kleine-Weber, H., Schroeder, S., Krüger, N., Herrler, T., Erichsen, S., Schiergens, T.S., Herrler, G., Wu, N.H., Nitsche, A., Müller, M.A., Drosten, C., Pöhlmann, S., 2020b. SARS-CoV-2 cell entry depends on ACE2 and TMPRSS2 and is blocked by a clinically proven protease inhibitor. *Cell* 181, 271–280. <https://doi.org/10.1016/j.cell.2020.02.052> e8.
- Hu, J., He, C.L., Gao, Q., Zhang, G.J., Cao, X.X., Long, Q.X., Deng, H.J., Huang, L.Y., Chen, J., Wang, K., et al., 2020. The d614g Mutation of sars-cov-2 Spike Protein Enhances Viral Infectivity. *BioRxiv*.
- Huang, Y., Yang, C., Xu, X.F., Xu, W., Liu, S.W., 2020. Structural and functional properties of sars-cov-2 spike protein: potential antiviral drug development for covid-19. *Acta Pharmacol. Sin.* 41, 1141–1149.
- Hubbard, S.J., Thornton, J.M., 1993. Naccess. Computer Program, vol. 2. Department of Biochemistry and Molecular Biology, University College London.
- Humphrey, W., Dalke, A., Schulten, K., 1996. VMD: visual molecular dynamics. *J. Mol. Graph.* 14, 33–38. [https://doi.org/10.1016/0263-7855\(96\)00018-5](https://doi.org/10.1016/0263-7855(96)00018-5).
- Isabel, S., Graña-Miraglia, L., Gutierrez, J.M., Bundalovic-Torma, C., Groves, H.E., Isabel, M.R., Eshaghi, A., Patel, S.N., Gubbay, J.B., Poutanen, T., et al., 2020. Evolutionary and structural analyses of sars-cov-2 d614g spike protein mutation now documented worldwide. *Sci. Rep.* 10, 1–9.
- Jo, S., Song, K.C., Desaire, H., MacKerell Jr., A.D., Im, W., 2011. Glycan reader: automated sugar identification and simulation preparation for carbohydrates and glycoproteins. *J. Comput. Chem.* 32, 3135–3141.
- Ju, B., Zhang, Q., Ge, J., Wang, R., Sun, J., Ge, X., Yu, J., Shan, S., Zhou, B., Song, S., Tang, X., Yu, J., Lan, J., Yuan, J., Wang, H., Zhao, J., Zhang, S., Wang, Y., Shi, X., Liu, L., Zhao, J., Wang, X., Zhang, Z., Zhang, L., 2020. Human neutralizing antibodies elicited by SARS-CoV-2 infection. *Nature* 584, 115–119. <https://doi.org/10.1038/s41586-020-2380-z>.
- Kandt, C., Ash, W.L., Tieleman, D.P., 2007. Setting up and running molecular dynamics simulations of membrane proteins. *Methods* 41, 475–488. <https://doi.org/10.1016/j.jymeth.2006.08.006>.
- Kannan, S.R., Spratt, A.N., Cohen, A.R., Naqvi, S.H., Chand, H.S., Quinn, T.P., Lorson, C.L., Byrareddy, S.N., Singh, K., 2021. Evolutionary analysis of the delta and delta plus variants of the sars-cov-2 viruses. *J. Autoimmun.* 102715.
- Korber, B., Fischer, W.M., Gnanakaran, S., Yoon, H., Theiler, J., Abfalterer, W., Hengartner, N., Giorgi, E.E., Bhattacharya, T., Foley, B., Hastie, K.M., Parker, M.D., Partridge, D.G., Evans, C.M., Freeman, T.M., de Silva, T.I., McDanal, C., Perez, L.G., Tang, H., Moon-Walker, A., Whelan, S.P., LaBranche, C.C., Saphire, E.O., Montefiori, D.C., Angyal, A., Brown, R.L., Carrilero, L., Green, L.R., Groves, D.C., Johnson, K.J., Keeley, A.J., Lindsey, B.B., Parsons, P.J., Raza, M., Rowland-Jones, S., Smith, N., Tucker, R.M., Wang, D., Wyles, M.D., 2020. Tracking changes in SARS-CoV-2 spike: evidence that d614g increases infectivity of the COVID-19 virus. *Cell* 182, 812–827. <https://doi.org/10.1016/j.cell.2020.06.043> e19.
- Lan, J., Ge, J., Yu, J., Shan, S., Zhou, H., Fan, S., Zhang, Q., Shi, X., Wang, Q., Zhang, L., Wang, X., 2020. Structure of the SARS-CoV-2 spike receptor-binding domain bound to the ACE2 receptor. *Nature* 581, 215–220. <https://doi.org/10.1038/s41586-020-2180-5>.
- Liu, L., Wang, P., Nair, M.S., Yu, J., Rapp, M., Wang, Q., Luo, Y., Chan, J.F.W., Sahi, V., Figueroa, A., et al., 2020. Potent neutralizing antibodies against multiple epitopes on sars-cov-2 spike. *Nature* 584, 450–456.
- Liu, Z., VanBlargan, L.A., Bloyet, L.M., Rothlauf, P.W., Chen, R.E., Stumpf, S., Zhao, H., Errico, J.M., Theel, E.S., Liebeskind, M.J., et al., 2021. Identification of sars-cov-2 spike mutations that attenuate monoclonal and serum antibody neutralization. *Cell Host Microbe* 29, 477–488.
- Lok, S.M., 2021. An ntd supersite of attack. *Cell Host Microbe* 29, 744–746.
- Mansbach, R.A., Chakraborty, S., Nguyen, K., Montefiori, D.C., Korber, B., Gnanakaran, S., 2021. The sars-cov-2 spike variant d614g favors an open conformational state. *Sci. Adv.* 7, eabf3671.
- Mark, P., Nilsson, L., 2001. Structure and dynamics of the TIP3p, SPC, and SPC/e water models at 298 K. *J. Phys. Chem.* 105, 9954–9960. <https://doi.org/10.1021/jp003020w>.
- Martínez-Flores, D., Zepeda-Cervantes, J., Cruz-Reséndiz, A., Aguirre-Sampieri, S., Sampieri, A., Vaca, L., 2021. Sars-cov-2 vaccines based on the spike glycoprotein and implications of new viral variants. *Front. Immunol.* 12.
- McCallum, M., De Marco, A., Lempp, F.A., Tortorici, M.A., Pinto, D., Walls, A.C., Beltramello, M., Chen, A., Liu, Z., Zatta, F., et al., 2021. N-terminal domain antigenic mapping reveals a site of vulnerability for sars-cov-2. *Cell* 184, 2332–2347.
- Mittal, A., Manjunath, K., Ranjan, R.K., Kaushik, S., Kumar, S., Verma, V., 2020. Covid-19 pandemic: insights into structure, function, and hacc2 receptor recognition by sars-cov-2. *PLoS Pathog.* 16, e1008762.
- Mullick, B., Magar, R., Jhunjhunwala, A., Farimani, A.B., 2021. Understanding mutation hotspots for the sars-cov-2 spike protein using shannon entropy and k-means clustering. *Comput. Biol. Med.* 104915.
- Neher, R.A., Dyrda, R., Druelle, V., Hodcroft, E.B., Albert, J., 2020. Potential impact of seasonal forcing on a SARS-CoV-2 pandemic. *Swiss Med. Wkly.* <https://doi.org/10.1101/2020.02.13.20022806>.
- Okada, P., Buathong, R., Phuygun, S., Thanadachakul, T., Parmen, S., Wongboot, W., Waichareon, S., Wacharapluesadee, S., Uttayamakul, S., Vachiraphan, A., Chittaganpitch, M., Mekha, N., Janejai, N., Iamsirithaworn, S., Lee, R.T., Maurer-Stroh, S., 2020. Early transmission patterns of coronavirus disease 2019 (COVID-19) in travellers from wuhan to Thailand, january 2020. *Euro Surveill.* 25. <https://doi.org/10.2807/1560-7917.es.2020.25.8.2000097>.
- O'Toole, A., Scher, E., Underwood, A., Jackson, B., Hill, V., McCrone, J.T., Colquhoun, R., Ruis, C., Abu-Dahab, K., Taylor, B., et al., 2021. Assignment of epidemiological lineages in an emerging pandemic using the pangolin tool. *Virus Evol.* 30.
- Parrinello, M., Rahman, A., 1981. Polymorphic transitions in single crystals: a new molecular dynamics method. *J. Appl. Phys.* 52, 7182–7190. <https://doi.org/10.1063/1.328693>.
- Petersen, E.F., Goddard, T.D., Huang, C.C., Couch, G.S., Greenblatt, D.M., Meng, E.C., Ferrin, T.E., 2004a. UCSF chimera2a visualization system for exploratory research and analysis. *J. Comput. Chem.* 25, 1605–1612. <https://doi.org/10.1002/jcc.20084>.

- Pettersen, E.F., Goddard, T.D., Huang, C.C., Couch, G.S., Greenblatt, D.M., Meng, E.C., Ferrin, T.E., 2004b. Ucsf chimera—a visualization system for exploratory research and analysis. *J. Comput. Chem.* 25, 1605–1612.
- Pettersen, E.F., Goddard, T.D., Huang, C.C., Meng, E.C., Couch, G.S., Croll, T.I., Morris, J.H., Ferrin, T.E., 2021. Ucsf chimerax: structure visualization for researchers, educators, and developers. *Protein Sci.* 30, 70–82.
- Portelli, S., Olshansky, M., Rodrigues, C.H., D'Souza, E.N., Myung, Y., Silk, M., Alavi, A., Pires, D.E., Ascher, D.B., 2020. Exploring the structural distribution of genetic variation in sars-cov-2 with the covid-3d online resource. *Nat. Genet.* 52, 999–1001.
- Rambaut, A., Loman, N., Pybus, O., Barclay, W., Barrett, J., Carabelli, A., Connor, T., Peacock, T., Robertson, D.L., Volz, E., 2020. Preliminary Genomic Characterisation of an Emergent Sars-Cov-2 Lineage in the UK Defined by a Novel Set of Spike Mutations. *Rees-Spear, C., Muir, L., Griffith, S., Heaney, J., Aldon, Y., Snitselaar, J., Thomas, P., Graham, C., Seow, J., Lee, N., Rosa, A., Roustan, C., Houlihan, C., Sanders, R., Gupta, R., Cherepanov, P., Stauss, H., Nastouli, E., Doores, K., van Gils, M., McCoy, L., 2021. The impact of spike mutations on SARS-CoV-2 neutralization. Cell Rep. <https://doi.org/10.1101/2021.01.15.426849>.*
- Resende, P.C., Bezerra, J.F., Vasconcelos, R., Arantes, I., Appolinario, L., Mendonça, A.C., Paixao, A.C., Rodrigues, A.C.D., Silva, T., Rocha, A.S., et al., 2021. Spike e484k mutation in the first Sars-Cov-2 reinfection case confirmed in Brazil, 2020. *Virological* 10 [Internet].
- Schrödinger, L.L.C., 2015. The PyMOL Molecular Graphics System, Version 1.8.
- Shang, J., Ye, G., Shi, K., Wan, Y., Luo, C., Aihara, H., Geng, Q., Auerbach, A., Li, F., 2020. Structural basis of receptor recognition by sars-cov-2. *Nature* 581, 221–224.
- Shapovalov, M.V., Dunbrack Jr., R.L., 2011. A smoothed backbone-dependent rotamer library for proteins derived from adaptive kernel density estimates and regressions. *Structure* 19, 844–858.
- Shu, Y., McCauley, J., 2017. GISAID: global initiative on sharing all influenza data – from vision to reality. *Euro Surveill.* 22. <https://doi.org/10.2807/1560-7917.es.2017.22.13.30494>.
- Starr, T.N., Greaney, A.J., Hilton, S.K., Ellis, D., Crawford, K.H., Dingens, A.S., Navarro, M.J., Bowen, J.E., Tortorici, M.A., Walls, A.C., et al., 2020. Deep mutational scanning of sars-cov-2 receptor binding domain reveals constraints on folding and ace2 binding. *Cell* 182, 1295–1310.
- Tegally, H., Wilkinson, E., Giovanetti, M., Iranzadeh, A., Fonseca, V., Giandhari, J., Doolabh, D., Pillay, S., San, E.J., Msomi, N., et al., 2020. Emergence and Rapid Spread of a New Severe Acute Respiratory Syndrome-Related Coronavirus 2 (Sars-cov-2) Lineage with Multiple Spike Mutations in South Africa. *medRxiv*.
- Tegally, H., Wilkinson, E., Giovanetti, M., Iranzadeh, A., Fonseca, V., Giandhari, J., Doolabh, D., Pillay, S., San, E.J., Msomi, N., et al., 2021. Detection of a sars-cov-2 variant of concern in South Africa. *Nature* 592, 438–443.
- Teruel, N., Mailhot, O., Najmanovich, R.J., 2021. Modelling conformational state dynamics and its role on infection for sars-cov-2 spike protein variants. *PLoS Comput. Biol.* 17, e1009286.
- Tiberti, M., Invernizzi, G., Lambrugh, M., Inbar, Y., Schreiber, G., Papaleo, E., 2014. Pyinteract: a framework for the analysis of interaction networks in structural ensembles of proteins. *J. Chem. Inf. Model.* 54, 1537–1551.
- Turoňová, B., Sikora, M., Schürmann, C., Hagen, W.J., Welsch, S., Blanc, F.E., von Bülow, S., Gecht, M., Bagola, K., Hörner, C., et al., 2020. In situ structural analysis of sars-cov-2 spike reveals flexibility mediated by three hinges. *Science* 370, 203–208.
- Volz, E., Hill, V., McCrone, J.T., Price, A., Jorgensen, D., O'Toole, Á., Southgate, J., Johnson, R., Jackson, B., Nascimento, F.F., et al., 2021. Evaluating the effects of sars-cov-2 spike mutation d614g on transmissibility and pathogenicity. *Cell* 184, 64–75.
- Walls, A.C., Park, Y.J., Tortorici, M.A., Wall, A., McGuire, A.T., Veesler, D., 2020. Structure, function, and antigenicity of the SARS-CoV-2 spike glycoprotein. *Cell* 181, 281–292. <https://doi.org/10.1016/j.cell.2020.02.058> e6.
- Wang, P., Casner, R.G., Nair, M.S., Wang, M., Yu, J., Cerutti, G., Liu, L., Kwong, P.D., Huang, Y., Shapiro, L., et al., 2021a. Increased resistance of sars-cov-2 variant p. 1 to antibody neutralization. *Cell Host Microbe* 29, 747–751.
- Wang, P., Nair, M.S., Liu, L., Iketani, S., Luo, Y., Guo, Y., Wang, M., Yu, J., Zhang, B., Kwong, P.D., et al., 2021b. Antibody resistance of sars-cov-2 variants b. 1.351 and b. 1.1. 7. *Nature* 593, 130–135.
- Wang, Y., Wang, L., Cao, H., Liu, C., 2021c. Sars-cov-2 s1 is superior to the rbd as a covid-19 subunit vaccine antigen. *J. Med. Virol.* 93, 892–898.
- Weisblum, Y., Schmidt, F., Zhang, F., DaSilva, J., Poston, D., Lorenzi, J.C., Muecksch, F., Rutkowska, M., Hoffmann, H.H., Michailidis, E., et al., 2020. Escape from neutralizing antibodies by sars-cov-2 spike protein variants. *Elife* 9, e61312.
- Wen, F., Yu, H., Guo, J., Li, Y., Luo, K., Huang, S., 2020. Identification of the hyper-variable genomic hotspot for the novel coronavirus sars-cov-2. *J. Infect.* 80, 671.
- West Jr., A.P., Wertheim, J.O., Wang, J.C., Vasylyeva, T.I., Havens, J.L., Chowdhury, M.A., Gonzalez, E., Fang, C.E., Di Lonardo, S.S., Hughes, S., et al., 2021. Detection and Characterization of the Sars-Cov-2 Lineage B. 1.526 in New York. *bioRxiv*.
- Wrobel, A.G., Benton, D.J., Xu, P., Roustan, C., Martin, S.R., Rosenthal, P.B., Skehel, J.J., Gamblin, S.J., 2020. Sars-cov-2 and bat ratg13 spike glycoprotein structures inform on virus evolution and furin-cleavage effects. *Nat. Struct. Mol. Biol.* 27, 763–767.
- Xia, S., Lan, Q., Su, S., Wang, X., Xu, W., Liu, Z., Zhu, Y., Wang, Q., Lu, L., Jiang, S., 2020. The role of furin cleavage site in sars-cov-2 spike protein-mediated membrane fusion in the presence or absence of trypsin. *Signal Transduct. Targeted Ther.* 5, 1–3.
- Yan, R., Zhang, Y., Li, Y., Ye, F., Guo, Y., Xia, L., Zhong, X., Chi, X., Zhou, Q., 2021. Structural basis for the different states of the spike protein of sars-cov-2 in complex with ace2. *Cell Res.* 31, 717–719.
- Yang, T.J., Yu, P.Y., Chang, Y.C., Liang, K.H., Tso, H.C., Ho, M.R., Chen, W.Y., Lin, H.T., Wu, H.C., Hsu, S.T.D., 2021. Effect of sars-cov-2 b. 1.1. 7 mutations on spike protein structure and function. *Nat. Struct. Mol. Biol.* 28, 731–739.
- Yurkovetskiy, L., Wang, X., Pascal, K.E., Tomkins-Tinch, C., Nyalile, T.P., Wang, Y., Baum, A., Diehl, W.E., Dauphin, A., Carbone, C., Veinotte, K., Egri, S.B., Schaffner, S.F., Lemieux, J.E., Munro, J.B., Rafique, A., Barve, A., Sabeti, P.C., Kyratsous, C.A., Dudkina, N.V., Shen, K., Luban, J., 2020. Structural and functional analysis of the d614g SARS-CoV-2 spike protein variant. *Cell* 183, 739–751. <https://doi.org/10.1016/j.cell.2020.09.032> e8.
- Zahradnik, J., Marciano, S., Shemesh, M., Zoler, E., Chiaravalli, J., Meyer, B., Dym, O., Elad, N., Schreiber, G., 2021. Sars-cov-2 Rbd in Vitro Evolution Follows Contagious Mutation Spread, yet Generates an Able Infection Inhibitor. *bioRxiv*.
- Zhang, J., Cai, Y., Xiao, T., Lu, J., Peng, H., Sterling, S.M., Walsh, R.M., Rits-Volloch, S., Zhu, H., Woosley, A.N., et al., 2021. Structural impact on sars-cov-2 spike protein by d614g substitution. *Science* 372, 525–530.
- Zhang, L., Jackson, C.B., Mou, H., Ojha, A., Peng, H., Quinlan, B.D., Rangarajan, E.S., Pan, A., Vanderheiden, A., Suthar, M.S., et al., 2020. Sars-cov-2 spike-protein d614g mutation increases virion spike density and infectivity. *Nat. Commun.* 11, 1–9.
- Zhu, X., Mannar, D., Srivastava, S.S., Berezuk, A.M., Demers, J.P., Saville, J.W., Leopold, K., Li, W., Dimitrov, D.S., Tuttle, K.S., et al., 2021. Cryo-electron microscopy structures of the n501y sars-cov-2 spike protein in complex with ace2 and 2 potent neutralizing antibodies. *PLoS Biol.* 19, e3001237.
- Zimmerman, M.I., Porter, J.R., Ward, M.D., Singh, S., Vithani, N., Meller, A., Mallimadugula, U.L., Kuhn, C.E., Borowsky, J.H., Wiewiora, R.P., et al., 2021. Sars-cov-2 simulations go exascale to predict dramatic spike opening and cryptic pockets across the proteome. *Nat. Chem.* 1–9.